

Ion-photon entanglement and quantum frequency conversion with trapped Ba⁺ ions

J. D. Siverns, X. Li and Q. Quraishi*

Army Research Laboratory, Adelphi, MD 20783 and

*Joint Quantum Institute, University of Maryland, College Park, MD 20742**

(Dated: compiled October 18, 2021)

Trapped ions are excellent candidates for quantum nodes, as they possess many desirable features of a network node including long-lifetimes, on-site processing capability and produce photonic flying qubits. However, unlike classical networks in which data may be transmitted in optical fibers and the range of communication readily extended with amplifiers, quantum systems often emit photons that have limited propagation range in optical fibers and, by virtue of the nature of a quantum state, cannot be noiselessly amplified. Here, we first describe a method to extract flying qubits from a Ba⁺ trapped ion via shelving to a long lived, low-lying D-state with higher entanglement probabilities compared with current strong and weak excitation methods. We show a projected fidelity of $\approx 89\%$ of the ion-photon entanglement. We compare several methods of ion-photon entanglement generation and show how the fidelity and entanglement probability varies as a function of the photon collection optic's numerical aperture. We then outline an approach for quantum frequency conversion of the photons emitted by the Ba⁺ ion to the telecom range for long-distance networking and to 780 nm, for potential entanglement with Rubidium based quantum memories. Our approach is significant for extending the range of quantum networks and for development of hybrid quantum networks comprised of different types of quantum memories.

PACS numbers:

I. INTRODUCTION

Trapped ions are a well-established system in which many of the desirable features for quantum information processing have been demonstrated [1], such as long-lived quantum coherence [2, 3] and storage and retrieval of quantum states using photons on scalable platforms [4]. From the first work [5] demonstrating a quantum gate with one trapped ion to the engineering of quantum states with 14 ions [6], efforts are now underway to establish networks of remotely situated trapped ion systems [7]. Two quantum nodes are connected when entanglement has been established via a joint measurement of single photons (flying qubits), emitted by each quantum node separately [8]. The nodes act as quantum memories, emitting photons entangled with the ion's internal state [9]. Entanglement between nodes can be established via Bell-state measurements. Such quantum networks may be used for teleportation between the nodes, even if there is no a-priori knowledge of the state to be teleported [10]. Lab-based networks connected by approximately 1 km optical fibers have demonstrated entanglement but the flying qubit wavelengths are incommensurate with low loss, long-distance propagation in optical fiber [11]. Modern telecommunication (telecom) networks utilize well-established networks of optical fibers linking remotely situated nodes. Unlike classical approaches to extending these data ranges using optical amplifiers, quantum information can neither be cloned nor noiselessly ampli-

fied [12], however, two-node entanglement swapping can serve as a quantum repeater to transfer quantum information [13].

It would be advantageous if emerging quantum networks could exploit existing telecom optical fiber infrastructures. In this case, long-distance quantum networking requires photonic flying qubits at telecom wavelengths for low-loss transmission. However, trapped ions, similar to other types of quantum memories like neutral atoms or nitrogen vacancy centers, typically emit photons which have high attenuation when propagated in optical fibers, as such memories emit either in the ultraviolet (UV), visible or near-IR regime. Optical frequency conversion via nonlinear processes is well established and may be used to obtain more desirable wavelengths. Quantum frequency conversion (QFC)[14] of single photons has been demonstrated using atomic vapors [15], photonic crystal fibers [16] and crystals such as lithium niobate [17, 18]. Recent work has shown QFC into telecom wavelengths from single photons emitted by quantum memories such as quantum dots [19] and neutral atoms [20]. Importantly, the quantum nature of the photon is preserved in the quantum frequency conversion process [14, 20, 21]. In addition, creating entanglements between different types of memories in a hybrid quantum network allows for each system's unique properties to be utilized [22]. Here, we present an approach to extract polarization entangled photonic flying qubits from a ¹³⁸Ba⁺ trapped ion memory and outline a scheme for quantum frequency conversion for long-distance and hybrid quantum networking.

*Electronic address: *qudsia.quraishi.civ@mail.mil

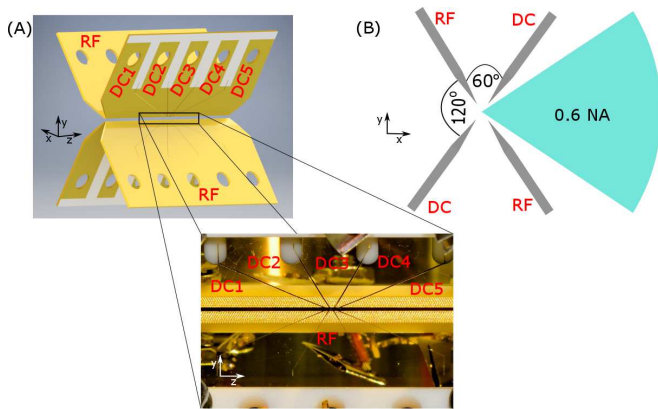


FIG. 1: (a) Schematic of the blade trap. The distance between the upper (segmented into five static voltage electrodes) and lower (RF) blades is $\sim 260 \mu\text{m}$ and the width of the central electrode (labeled DC3) is $\sim 250 \mu\text{m}$ at its tip. For illustration purposes, the inset shows a close up photograph of the trap with more detail of the electrode segmentation. The segments of the rf blade they are electrically shorted together creating one electrode. (b) Diagram showing the trap geometry in the x-y plane with the light cone of the 0.6 NA lens (half-angle of around 37°) shown in blue.

II. ION TRAPPING AND PHOTON EXTRACTION

Trapped ions confined in radio frequency (RF) Paul traps are versatile quantum systems from which flying qubits may be extracted with a high quantum correlation between the trapped ion memory and flying qubit [9]. Such systems have applications in frequency standards [23, 24], quantum information processing [4, 25, 26], quantum simulations [27–30] and quantum networking [31–33]. Networking two-individual nodes has been implemented over a distance of meters [8, 34, 35]. Here, we propose a method for near deterministic ion-photon entanglement production using continuous wave (CW) excitation and compare this approach to methods using strong [36] and weak excitation [9]. Strong excitation methods require a laser pulse with sufficient intensity to excite the ion with near unity probability. Typically, this is achieved with the use of a modelocked pulse laser [36]. The approach outlined here has a higher entanglement probability compared with both strong and weak excitation schemes [9, 37, 38]. The fidelity, although lower than other schemes, provides a higher entanglement probability which could be used for the demonstration of a proof-of-principle quantum network node without the need for additional experimental overhead involved with strong excitation schemes.

A. Ion trapping background

RF voltages applied to trap electrodes provide a suitable ponderomotive pseudo-potential to trap ions of

mass, m , and charge, e , which, for a linear Paul trap, is given by [39, 40]

$$\psi = \frac{e^2 V_0^2 \eta^2}{4mr^4 \Omega_{RF}^2} (x^2 + y^2), \quad (1)$$

where $\Omega_{RF}/2\pi$ is the RF frequency, r is the ion-electrode distance and V_0 is the amplitude of the RF voltage applied to the trap. Confinement of the ion along the z-axis can be achieved by the introduction of a potential in this direction created from various static voltage electrodes. The geometric factor η [40] is equal to one for a perfectly hyperbolic electrode geometry and less than one as the geometry strays from this perfect form. Ions trapped in this pseudo-potential will undergo secular motion with a frequency given by [39, 40]

$$\omega_s = \frac{eV_0\eta}{\sqrt{2mr^2\Omega_{RF}}}. \quad (2)$$

We use a linear four-blade trap as shown in Fig. 1(a). Such traps possess a node in the ponderomotive potential along the axis of the trap allowing either a single ion or a chain of ions to be trapped. Confinement along this node is provided by applying static voltages to the outer segments of the electrodes. These traps typically have depths of 1 eV to 10 eV, corresponding to $\approx 10^5 \text{K}$. It is possible to achieve ion temperatures of approximately 1 mK by applying a single laser cooling beam with momentum projections in all three motional directions of the ion. Hence, the ion can remain tightly confined in the trap allowing for repeated interrogation by optical beams for single photon production.

To increase the ion-photon entanglement probability, collection optics must capture as much spontaneously emitted light as possible. We have custom-designed our apparatus with a particularly high collection aperture optic. The physical arrangement of the blades allows for collection up to $\approx 10\%$ (numerical aperture (NA) of 0.6) of the light emitted from ions in the trap as shown in Fig. 1(b). Similar lenses integrated with blade-traps have substantially improved ion-photon entanglement probabilities [35].

B. Ion state preparation and ion-photon entanglement

A qubit is represented by the two Zeeman levels in the $S_{1/2}$ ground state of a $^{138}\text{Ba}^+$ ion with $|0\rangle = |m_j = -1/2\rangle$ and $|1\rangle = |m_j = +1/2\rangle$ as shown in Fig. 2(a). The ground state, $S_{1/2}$, is split into two Zeeman levels by applying a magnetic field which defines the direction of the quantization axis. It is possible, as we show below, to produce a single 493 nm photon with its polarization entangled with the qubit states $|1\rangle$ and $|0\rangle$ via shelving in the $D_{3/2}$ level. The $D_{3/2}$ level is long-lived (lifetime of 80 sec) allowing for effective shelving.

The ion-photon entanglement is produced using the following three steps. Firstly, the ion is initialized into the $m_j = +3/2$ ($m_j = -3/2$) state in the $D_{3/2}$ level, using π -polarized 493 nm light along with π and σ^+ (σ^-) polarized 650 nm CW lasers. Secondly, the ion is excited from the $D_{3/2}$ state to the $P_{1/2}$ state via a σ^- (σ^+) polarized 650 nm beam. Initially, the ion is only excited to the $P_{1/2}$ state Zeeman level $m_j = +1/2$ ($m_j = -1/2$). The effects of multiple excitations, including those to the opposite Zeeman level will be discussed in section II C 1. Finally, the ion can spontaneously decay from the excited state, $P_{1/2}$, to the ground state, $S_{1/2}$, via two dipole-transition allowed paths corresponding to either a π or σ^+ polarized photon. Observation in the direction perpendicular to the quantization axis means it is possible to view σ^\pm and π photons as horizontal $|H\rangle$ and vertical $|V\rangle$ polarizations respectively, yielding an ion-photon entangled state given by

$$|\Psi_G\rangle = \frac{1}{\sqrt{2}} |V\rangle |1\rangle + \frac{1}{\sqrt{2}} |H\rangle |0\rangle. \quad (3)$$

The state given by Eqn. 3 takes into account both the intensity pattern of the emitted σ^+ and π polarizations, with the latter being greater by a factor of two when the spherical polar angle, θ , of the emitted photons, with respect to the dipole axis, is equal to $\pi/2$. Also included are the Clebsch-Gordan coefficients of the transitions, shown in Fig. 3(a).

This intensity pattern difference arises from our observation direction with respect to the quantization axis. Photons emitted from the $P_{1/2}$ to $S_{1/2}$ transition have the unnormalised polarization states, $|\pi\rangle$ and $|\sigma^\pm\rangle$, which are given by

$$|\pi\rangle = -\sin\theta |\hat{\theta}\rangle \quad (4)$$

and

$$|\sigma^\pm\rangle = \frac{e^{\pm i\phi}}{\sqrt{2}} \left(\cos\theta |\hat{\theta}\rangle \pm i |\hat{\phi}\rangle \right) \quad (5)$$

respectively, where ϕ is the azimuthal angle with respect to the dipole axis and $\hat{\theta}$ and $\hat{\phi}$ are the respective unit vectors. It can be seen from Eqns. 4 and 5 that when the angle θ is set to $\pi/2$ the two polarisations are orthogonal [9] and, after taking into account the relevant Clebsch-Gordan coefficients, we obtain Eqn.3.

It should be noted that initialization into the opposite Zeeman level of the $D_{3/2}$ ($m_j = -3/2$) is driven by σ^+ polarization of the 650 nm beam. This results in coupling to the $m_j = -1/2$ Zeeman level in the $P_{1/2}$ level and produces an ion-photon entangled state given by

$$|\Psi_B\rangle = \frac{1}{\sqrt{2}} |H\rangle |1\rangle + \frac{1}{\sqrt{2}} |V\rangle |0\rangle. \quad (6)$$

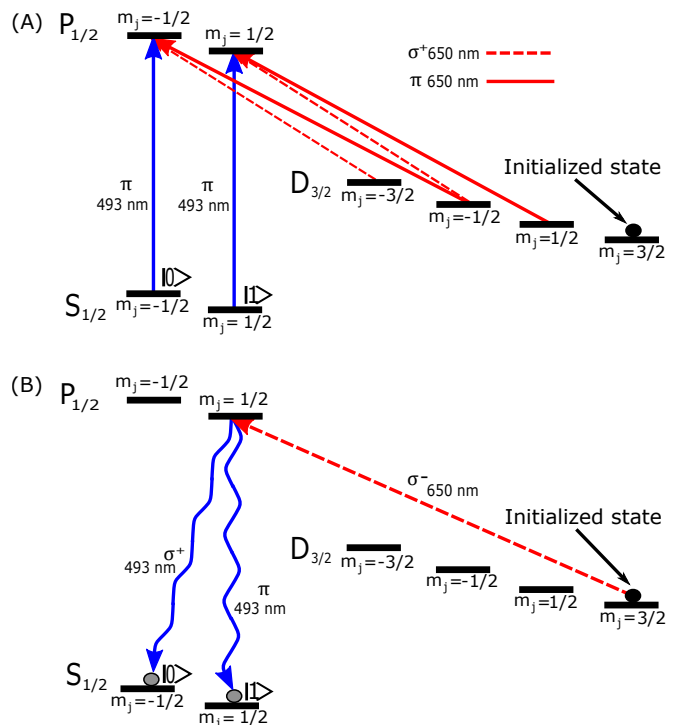


FIG. 2: (a) The transitions required for initializing a $^{138}\text{Ba}^+$ ion in the $m_j = +3/2$ state in the $D_{3/2}$ level. (b) The 650 nm σ^- transition required for the generation of the 493 nm photon and production of the ion-photon entangled state given in equation 3.

The flying qubit in this state carries with it information about the atom's state, meaning that a measurement of one polarization correlates to a particular atomic state. Interference between photons from a similarly prepared remote quantum memory node would generate entanglement between the two nodes, forming a quantum network. Two prominent factors which would degrade the purity of the ion-photon entangled state include re-excitation from the $D_{3/2}$ level and polarization mixing, as discussed in sections II C 1 and II C 2 respectively.

C. Fidelity of ion-photon entanglement

The target state given by Eqn. 3, is produced by decay from the $m_j = 1/2$ state of the $P_{1/2}$ level to the two $S_{1/2}$ ground states via two paths with Clebsch-Gordan coefficients shown in Fig. 3(a) (solid blue line). Factors which degrade the purity of the ion-photon entanglement include re-excitation from the $D_{3/2}$ level and polarization mixing due to the large collection angle. In the former case, rather than a pure state, a mixed state is obtained affecting the ability of the scheme to generate the desired entanglement. A common measure of the extent to which the desired target state is obtained is given by the fidelity. Below we analyze the fidelity under re-excitation and polarization mixing.

1. Effect of multiple excitations on state fidelity

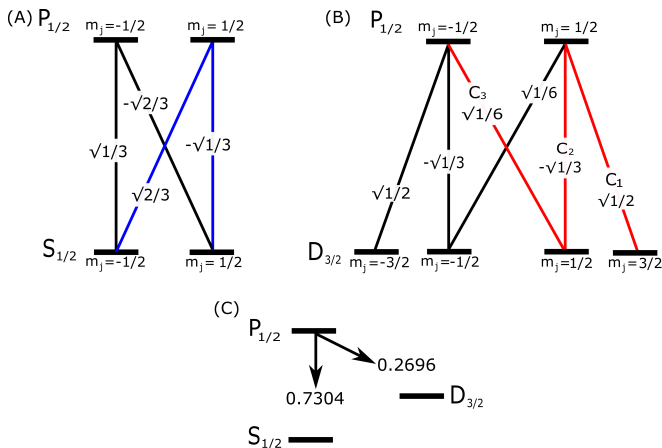


FIG. 3: Diagram showing the Clebsch-Gordan coefficients for transitions between the (a) ground-state $S_{1/2}$ and $P_{1/2}$ levels and (b) the $P_{1/2}$ and meta-stable $D_{3/2}$ level. (c) A simplified energy level diagram showing the branching ratio from the excited $P_{1/2}$ level to the $S_{1/2}$ and the $D_{3/2}$ level [41].

The excitation scheme presented here (Fig. 2) is unlike some [9, 37] used for ion-photon entanglement as the excitation (at 650 nm) is at an entirely different wavelength than the emitted photon (at 493 nm). This is clearly advantageous in terms of filtering background light, but also serves to improve ion-photon entanglement probabilities. Re-attempts at successful entanglement can occur after failed attempts during the same experiment cycle, albeit at the expense of the fidelity.

The ratio of a CW pulse duration, Δt , to the natural linewidth, τ , gives the probability of double excitation, $p_\gamma = 1 - \exp(-\Delta t/\tau)$. If we assume a worst case scenario of continuous ($\Delta t \rightarrow \infty$) exposure to 650 nm σ^- light, then $p_\gamma \rightarrow 1$. The re-excitation occurs because there is an appreciable probability (approximately 27%, see Fig. 3) of the ion decaying back to the $D_{3/2}$ manifold, although not exclusively into the initialized state shown in Fig. 2(a). The decay back to the $D_{3/2}$ manifold happens via three possible channels emitting either a σ^+ , σ^- or π photon, with the Clebsch-Gordan (C-G) coefficients shown in Fig. 3 [41].

If the ion decays back to the initialized state shown in Fig. 2(a), we would proceed as already described in Section II B without any effect on the fidelity. If the decay is via a π photon (to the $m_j = +1/2$ Zeeman level, with C-G coefficient of $-\sqrt{1/3}$) then the subsequent 650 nm excitation will be to the $m_j = -1/2$ Zeeman level of the $P_{1/2}$ state. Any 493 nm decay to the ground state will result in the ion-photon entangled state given by Eqn. 6 being created instead of the desired state given by Eqn. 3. If the decay is via a σ^+ photon (to the $m_j = -1/2$ level, with C-G coefficient $\sqrt{1/6}$), the ion will go dark and no ion-photon entanglement will occur. Therefore, the ion-

photon entanglement created with this scheme will be given by the mixed state

$$\Psi_m = \frac{P_G}{P_G + P_B} |\Psi_G\rangle + \frac{P_B}{P_G + P_B} |\Psi_B\rangle \quad (7)$$

where P_G and P_B are the probabilities of the scheme creating the ion-photon entangled states $|\Psi_G\rangle$ and $|\Psi_B\rangle$ respectively, and are given by the following geometric series

$$P_G = \frac{Br_{493}}{1 - (C_1^2 Br_{650})} \approx 0.844 \quad (8)$$

$$P_B = \frac{Br_{493} Br_{650} C_2^2}{1 - (C_3^2 Br_{650})} \approx 0.103. \quad (9)$$

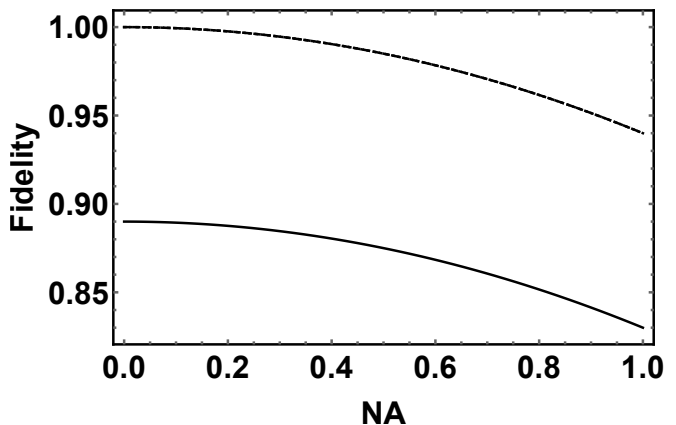


FIG. 4: The fidelity of the ion-photon entangled state as a function of NA is shown for the scheme outlined in Section II B (solid), weak and strong (both dashed) excitation methods. The weak and strong excitation methods fall on the same upper (dashed) curve.

Here Br_{493} and Br_{650} are the branching ratios from the $P_{1/2}$ state to the ground state and $D_{3/2}$ state respectively, and C_1 , C_2 and C_3 are the C-G coefficients of the decays shown in Fig. 3. This means that a 493 nm photon will be emitted by the ion with a success of $\approx 94.7\%$, making the scheme near deterministic, albeit with a lower fidelity for the target state when compared with weak and strong excitation methods as shown in Fig. 4. When unsuccessful, the ion will have been pumped into a dark state in the $D_{3/2}$ level.

Here, we examine the effect of these re-excitations by using the metric of fidelity, defined as [42]

$$F = \langle \Psi | \rho | \Psi \rangle, \quad (10)$$

where $|\Psi\rangle$ is the intended pure state and ρ is the density matrix of the created state. The fidelity of the mixed state, Ψ_m , created by this scheme with the intended pure

state, Ψ_G , can be calculated to be ≈ 0.89 . Although this scheme yields a lower fidelity than standard strong and weak excitation methods (both can achieve fidelities near to unity), it allows the user to produce ion-photon entanglement with a higher probability and in the case of the strong excitation method, without the need for additional pulsed laser apparatus. By adopting this method we will have the ability to perform proof-of-principle quantum networking experiments with quantum frequency conversion of the emitted photon.

2. Effect of polarization mixing due to collection solid-angle on state fidelity

Ion-photon entanglement is useful as a resource for quantum networking, as the photon carries information about the atomic state to a remote site. To optimize networking protocols we wish to capture photons from as many entanglement trials as possible. However, the photon is emitted from the $P_{1/2}$ level spontaneously into the full solid angle 4π . There are a variety of approaches to optimize collection including optical cavities [43, 44] and in-vacu [45, 46] and ex-vacu [35] high NA lenses. High NA lenses can have such a large collection angle that the σ^\pm polarized light typically has a projection on the π polarized light when viewed in a horizontal and vertical polarization basis. Here we examine how this projection reduces the fidelity of the ion-photon entanglement.

We plan to integrate an ex-vacu 0.6 NA lens into our setup which is designed to collect approximately 10% of the light and is AR coated for both 493 nm and 650 nm. Ex-vacu high NA collection reduces complexity of the in-vacuum trap assembly and readily allows for optical corrections with additional free-space optics. Although, in-vacuo optics can provide a more modular, compact and scalable solution for future nodes of a potential quantum network [45, 47]. The analysis below holds for both types of lenses.

The fraction of emitted photons collected by a lens with numerical aperture, NA, is given by

$$\frac{\Omega}{4\pi} \approx \frac{1}{4}\text{NA}^2. \quad (11)$$

From Eqn. 11 it is clear to see that a lens with a high NA will result in the collection of a higher fraction of the photons emitted from an atom. However, as can be seen in Eqns. 4 and 5, if the spherical polar angle, θ , is not equal to $\pi/2$ then there will be a loss of orthogonality between the σ and π light emitted from the atom, when viewed in a Cartesian basis. In this case, the fidelity of the collected ion-photon entangled state varies from the ideal ion-photon entangled state. For CW excitation of the ion as outlined in IIB, the fidelity of the entangled state as a function of the collection lens's NA (Fig. 4, solid trace) is given by [9]

$$F = F_{\text{max}} - 0.24(\Omega/4\pi) \approx F_{\text{max}} - 0.24\left(\frac{1}{4}\text{NA}^2\right) \quad (12)$$

where F_{max} is the maximum fidelity achievable. For the method outlined in section IIB, the fidelity $F_{\text{max}} \approx 0.89$, so we obtain a fidelity $F_{0.6} = 0.87$ for NA = 0.6. For comparison, also shown are curves for a weak excitation method [37] and a strong excitation method [36] (dashed line). Both have the same fidelity as both have F_{max} near unity.

The approach presented here does not reach the high fidelities (unity with a NA of zero) achieved with these other two schemes, however, it does yield a higher probability of entanglement compared to the other two schemes as shown below. For improved fidelities, achieved by avoiding multiple excitations, using a single pulse from a pulsed laser is a desirable approach even though the entanglement probability is reduced.

3. Probability of ion-photon entanglement with $D_{3/2}$ initialization

Using a high NA lens increases the probability of photon capture and hence, the ion-photon entanglement probability. This higher entanglement probability is shown in Fig. 5 and is given by

$$P = P_e P_s \frac{\text{NA}^2}{4} \quad (13)$$

where P_e is the probability of excitation to the P-level and P_s is the probability of decay to the S-level. For the curves shown, the weak and strong excitation methods have P_e equal to 0.2 and 1 respectively and both have P_s equal to 0.7304, set by the branching ratio [Fig. 3(c)]. For the method outlined in Section IIB where we initialize in the $D_{3/2}$ level, the product, $P_e P_s = 0.947$ (as shown in Section IIC 1) meaning re-excitation increases the probability of obtaining an entangled state. For an NA = 0.6 an ion-photon entanglement probability of $P = 0.085$ can be obtained. It is notable that the excitation scheme outlined in Section B has a reasonable fidelity but the highest entanglement probability. For proof-of-principle experiments this would be appropriate to transmit quantum information to a remote site.

TABLE I: Comparison of excitation schemes with fidelity, $F_{0.6}$, and ion-photon entanglement generation probability, $P_{0.6}$, evaluated at NA=0.6.

Excitation scheme	$P_e P_s$	$P_{0.6}$	Fidelity, $F_{0.6}$
$D_{3/2}$ excitation	0.947	0.085	0.87
Weak excitation	0.146	0.014	0.98
Strong excitation	0.730	0.068	0.98

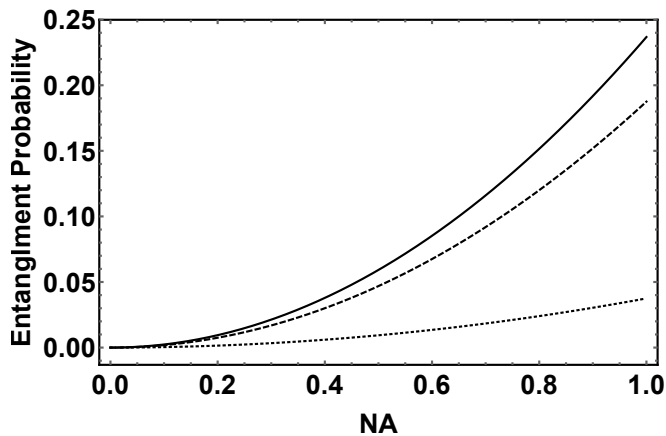


FIG. 5: The entanglement probability of the scheme outlined in Section IIB (solid), weak excitation method (dotted) and strong excitation method (dashed) as a function of NA.

III. QUANTUM FREQUENCY CONVERSION OF SINGLE PHOTONS

Trapped ions can serve as excellent quantum memories, however, they often emit in optical frequency ranges that have substantial attenuation even in dedicated wavelength-specific optical fibers. For instance, Yb^+ ions are highly desirable qubits, but they emit photons at 369 nm which have approximately 70 dB/km attenuation in commercially available single mode fibers. Although Ba^+ wavelengths (493nm, 650 nm) have improved fiber transmission over this Yb^+ emission wavelength, there is still substantial attenuation, as shown in Fig. 6.

Quantum frequency conversion [14] may be implemented to convert photons from the ion into the telcomm regime for low loss propagation through optical fibers therefore extending the range of quantum networking from lab-based two-node setups [36, 48]. Additionally, spectrally mismatched photons may be frequency converted to establish a hybrid quantum network comprised of two different types of quantum memories [49]. The frequency conversion must preserve the quantum properties and indeed, QFC experiments of single photons have shown that the quantum state of the single photon was preserved after QFC [16, 17].

Here, we present an approach for QFC of Ba^+ ion photons emitted at 493 nm and 650 nm. The 493 nm photons will be converted into the near infra-red (NIR) regime for potential networking with a neutral atom based quantum memory and the 650 nm photons will be converted into the telecom regime for long-distance quantum information transmission.

A. Quantum frequency conversion (QFC) background

Quantum frequency conversion [14] is a nonlinear process and relies on parametric oscillations of a material's electronic susceptibility, χ . With sufficiently intense optical pump fields, the higher order components of χ begin to dominate and modulate the material's polarizability as a function of the applied field, given by

$$P_i = \varepsilon_0 \sum_j \chi_{ij}^{(1)} E_j + \varepsilon_0 \sum_{jk} \chi_{ijk}^{(2)} E_j E_k + \varepsilon_0 \sum_{jkl} \chi_{ijkl}^{(3)} E_j E_k E_l + \dots \quad (14)$$

where ε_0 is the free space electric permittivity, E_{ijkl} denotes the electric field, and χ^n is a rank $n + 1$ tensor.

In a media with a large $\chi^{(2)}$ coefficient, the second order term in Eqn. 14 can dominate with a strong pump field, allowing the non-linear three-wave mixing (TWM) process to occur. Here the generation of the frequency $\omega_2 = \omega_1 \pm \omega_p$ is expected, where ω_1 is the frequency of the light to be converted and ω_p is the frequency of the high intensity pump. The plus sign corresponds to sum frequency generation (SFG), or upconversion, while the minus sign means difference frequency generation (DFG), or downconversion. Examples of a TWM process include frequency doubling in lithium niobate (LN), beta-barium-borate (BBO) and lithium triborate (LBO) crystals where $\omega_p = \omega_1$ and $\omega_2 = 2\omega_1$. With quasi-phase matching (QPM), TWM can be achieved in periodically poled materials like lithium niobate and potassium titanyl phosphate (KTP) even when $\omega_p \neq \omega_1$.

It is also possible to perform four-wave mixing (FWM) in centrosymmetric media as the second order term in Eqn. 14 is zero due to symmetry and the third order $\chi^{(3)}$ term can dominate, when subject to two pump lasers of sufficient intensity. $\chi^{(3)}$ media such as silicon nitride (SiN) microresonators [50] and optical fibers can both support FWM [51]. Recent work in SiN [52] has shown conversion efficiencies on par with those observed in PPLNs, however, not at a low enough noise rate required for the relatively low photon rates emitted by atomic quantum memories.

Frequency conversion at the single photon level with sufficiently low dark counts has been shown using TWM in periodically poled waveguides [20]. Given expected photon data rates [35], we plan to use a TWM process for frequency conversion of the Ba^+ ion photons.

In the case of periodically poled materials suitable for TWM, the quasi-phase matching can be achieved when

$$k_1 - k_p - k_2 - 2\pi m/\Lambda = 0 \quad (15)$$

where $k_1 = \omega_1 n_1/c$, $k_2 = \omega_2 n_2/c$, $k_p = \omega_p n_p/c$, m is the poling order and Λ is the poling period. QPM is achieved by periodically-poling the material and yields more than an order of magnitude improved conversion efficiencies as

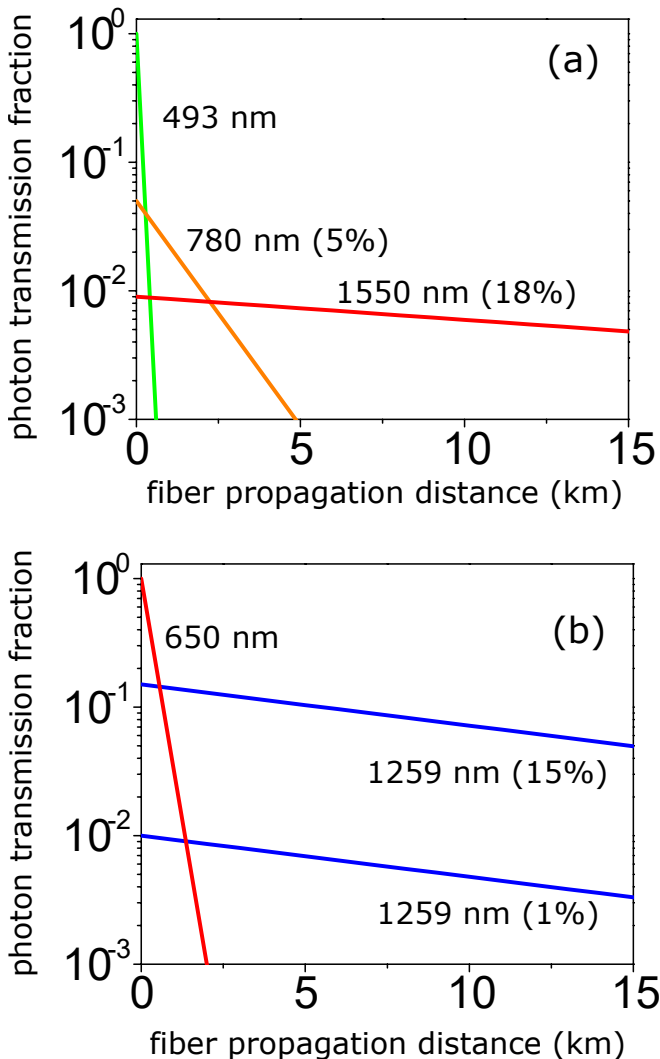


FIG. 6: Photon transmission fraction as a function of distance through wavelength specific fiber of photons derived from Ba^+ ions. Representative quantum frequency conversion efficiencies are given in parenthesis. (a) (green trace) Transmission of 493 nm photons with a fiber loss of -50 dB/km. (orange trace) Transmission of 780 nm photons with a fiber loss -3.5 dB/km, from frequency converted 493 nm photons. (red trace) Transmission of 1550 nm photons with a fiber loss -0.18 dB/km, from frequency converted 780 nm photons ($\sim 18\%$ QFC value reported in [20]) (b) (red trace) Transmission of 650 nm photons (fiber loss of -15 dB/km). (blue trace) Transmission of 1259 nm photons with a fiber loss of -0.3 dB/km from 650 nm photons.

compared against conversion using the largest coefficient that can be phase-matched with birefringence [53].

Most work in quantum frequency conversion has been done using TWM in periodically-poled lithium niobate (PPLN) because it can be readily engineered to yield high conversion efficiencies over a range of input wavelengths, especially with waveguides fabricated in them. Using a reverse proton exchange (RPE) technique [54] a waveguide may be buried beneath the surface of the bulk

crystal to reduce transmission loss and to ensure better spatial mode confinement of all the optical beams within the PPLN. Another desirable feature of these crystals are the observed low noise counts, suitable for the signal level emitted by atomic quantum memories [20].

Given that we are interested in converting and detecting single photons, noise photons at ω_1 and ω_2 must be minimized as they can spoil the ion-photon entanglement, considering current entanglement probabilities [35]. The primary sources of noise are spontaneous Raman scattering (SRS) and spontaneous parametric downconversion (SPDC). The SRS scattering can produce Raman peaks of noise sitting atop a noise pedestal. These effects are significantly minimized by ensuring ω_2 is greater than ω_p and by sufficient $\omega_2 - \omega_p$ detuning [18]. The SPDC noise may be minimized by ensuring that the pump wavelength is the longest wavelength in the TWM process [18] so that parasitic photons are produced at lower frequencies than either the input ω_1 or converted signal ω_2 . A final step in minimizing noise from the pump is done using optical filters, along with optical prisms and fiber Bragg gratings [20], to ensure that the background is significantly lower than the converted signal. Conversion of coherent light at 369 nm has been done to telecom wavelengths with a single-stage DFG process, but with ω_p greater than ω_2 [55], resulting in SPDC noise at the target telecom photon, and also in a two-stage process [56] with higher poling period and, therefore, reduced conversion efficiencies [57]. To observe a long-lived memory entangled with either a visible or telecom photon, it should be possible to generate local entanglement between Yb^+ and Ba^+ [58] and then do QFC on the photon emitted by the Ba^+ ion.

B. Proposed quantum frequency conversion for long distance and hybrid networking with Ba^+ ions

Ba^+ has two strong dipole transitions (493 nm, 650 nm) from the $P_{1/2}$ state. We begin by discussing frequency conversion of the 493 nm photons. In a single DFG stage, the 493 nm photon may be combined with a strong pump beam at 1343 nm ($\omega_p/2\pi = 223$ THz) to produce a photon at 780 nm ($\omega_2/2\pi = 384$ THz). This target wavelength is chosen to match the 780 nm D2 transition in neutral ^{87}Rb atoms. The pump laser may be frequency stabilized to match the 780 nm photon to the ^{87}Rb D2 transition. The similarity of the temporal profiles of the photons emitted from Ba^+ and Rb -based quantum memories, means that entanglement between them might be created via Bell state measurements [59], therefore creating a hybrid ion-neutral two-node quantum network that utilizes properties of each memory.

For long-distance communication through optical fibers, we can envisage using a second DFG conversion stage to convert the 780 nm photon to 1551 nm, with a pump at 1569 nm. Indeed, 780 nm photons from Rb -based quantum memories have already been converted

into the telecom regime [20, 60]. In Fig. 6(a) we show the propagation losses through wavelength specific fiber given conservative estimates on the QFC efficiencies. Given the high propagation loss of 493 nm in optical fiber, it is advantageous to do a single stage conversion efficiency to 780 nm for propagation over approximately 0.5 km even with a modest 5% QFC efficiency.

A Ba^+ ion's 650 nm ($\omega_1/2\pi = 461$ THz) photon can be converted into the telecom regime in a single DFG stage with the same CW pump laser at 1343 nm. The converted photon will be at 1259 nm ($\omega_2/2\pi = 238$ THz), near the beginning of the telecom o-band. Although there is a smaller probability of the ion emitting a 650 nm photon over a 493 nm photon (see Fig. 3), we only need a single DFG stage to obtain a telecom photon. However, two-stage conversion is also possible as shown in recent work of conversion from 650 nm to 1550 nm [61]. In Fig.6(b) we show the propagation losses through wavelength specific fiber of 650 nm and the target frequency converted photon given a modest conversion efficiency. Two different values of QFC efficiency are plotted to illustrate the crossing points between ω_1 and ω_2 at which conversion is beneficial. The approach outlined here for single-stage conversion of each Ba^+ ion allows for hybrid and long-distance quantum communication.

In Table II we summarize the relevant potential conversion possibilities. Although PPLN crystals have typically shown the best QFC performance, we will use PPKTP for the 493 nm conversion as it has a higher photorefractive damage threshold. The damage threshold is not relevant for single photon input to the PPKTP but is relevant for the coherent light levels needed for initial alignment.

TABLE II: QFC materials and frequencies

Conversion	$\omega_1/2\pi$ (THz)	$\omega_2/2\pi$ (THz)	$\omega_p/2\pi$ (THz)	Device
493 nm \rightarrow 780 nm	608	384	223	PPKTP
650 nm \rightarrow 1259 nm	461	238	223	PPLN
780 nm \rightarrow 1550 nm	384	193	191	PPLN

C. Planned experimental approach for visible photon frequency conversion

Previously we established a frequency converter setup for a neutral atom wavelength [62]. We can extend this approach to the Ba^+ wavelengths of interest here. To observe frequency conversion (and hence obtain the QFC conversion efficiency), we plan to use CW tunable external cavity diode laser (ECDL) sources. One ECDL is at the input frequency ω_1 (493 nm or 650 nm) and the other at the pump ω_p (1343 nm), seeding a single frequency Raman fiber amplifier. The seed laser can be locked to a transfer cavity, so that the converted photon is on resonance with the Rb transition.

For efficient coupling of both ω_1 and ω_p into the nonlinear waveguide, we plan to implement a free space scheme with a silver-coated, off-axis, parabolic mirror with a 15 mm focal length, as shown in Fig. 7. This gives us the ability to simultaneously couple the visible light and 1343 nm light into the respective fundamental modes of same waveguide [62]. Parabolic mirrors are excellent for focusing beams of vastly different wavelengths to the same spot, as they possess no chromatic aberration. Before the parabolic mirror, the two collimated beams are combined on a dichroic mirror that reflects signals at 493 nm or 650 nm and passes the 1343 nm pump. The waists of the beams are chosen to match the mode field diameter (MFD) of the fundamental mode of the relative color inside the waveguide.

To align the beams into the waveguide, we first put the two colors into a wavelength-division multiplexing (WDM) fiber combiner and put the output near the focus of the parabolic mirror. The output is then back-propagated through the setup. We adjust WDM along with the parabolic mirror on a 3-axis translation stage to collimate both colors simultaneously. We then separate the two colors with a dichroic mirror, and couple each beam into their relative fiber. As a result, if we send each color back through the fibers, they will be focused at the same spot after the parabolic mirror. The WDM is then exchanged with a nonlinear chip in a temperature controlled oven. By only adjusting the nonlinear chip's position with a 5-axis translation stage, we can couple both beams into the same waveguide.

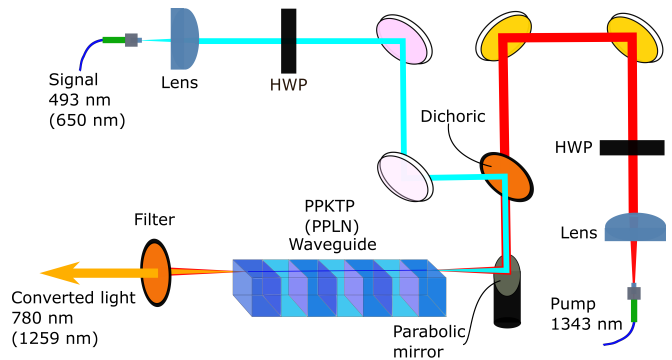


FIG. 7: Diagram showing the proposed DFG setup. The signal and pump beams are collimated out of each fiber with an aspheric lens. Their polarization are adjusted with half-wave plates (HWP) to vertical, i.e., perpendicular to the PPKTP chip surface with waveguides. The two beams are combined on a dichroic mirror before being simultaneously focused into the waveguide by a parabolic mirror. Residual pump and signal are filtered to allow measurement of the converted photons.

There are various free space coupling schemes that use other focusing optics, e.g., aspheric lens, grin lens, etc. However, in order to simultaneously couple both colors well, one either has to pre-shape one of the beams or to custom design the lens to be diffraction limited for both ω_1 and ω_p . It is also possible to write WDM waveguides

before the PPKTP/PPLN waveguide. This way, optical fibers carrying each color can be directly attached to the input of the corresponding WDM waveguide. Such miniaturized setups have excellent coupling efficiencies and are highly scalable. However, they are wavelength specific and typically not commercially available.

For QFC of single photons from the Ba^+ ion, the background noise from the pump laser needs to be carefully filtered. Narrow bandpass filters along with optical prisms and fiber Bragg gratings [20] can be used to ensure that the background is significantly lower than the converted signal. The final single photon detection can be performed with a superconducting nanowire single photon detector, which can achieve more than 95% quantum efficiency in the telecom regime [63].

D. Summary

Establishing a long-distance network using quantum memories involves entanglement generation between nodes. Photons entangled with quantum memories are excellent carriers of quantum information. Our approach to extract flying qubits from a Ba^+ ion provides high entanglement probabilities between the photon and ion compared with current weak and strong excitation schemes, however, at the loss of some fidelity. We showed

that although high numerical aperture lenses can improve the photon collection efficiency, they can act to degrade the quality of the ion-photon entanglement state due to polarization mixing. We proposed quantum frequency conversions of the Ba^+ ion wavelengths with only one pump laser to drive both conversion processes. The method outlined would produce photons available either for hybrid quantum networking or long-distance quantum communication utilizing existing telecom fiber networks.

IV. FUNDING INFORMATION

Funding provided by the Army Research Laboratory (ARL) under Cooperative Agreement (W911NF-14-2-0101) and ARL's Center for Distributed Quantum Information.

V. ACKNOWLEDGEMENTS

We thank Chris Monroe for the use of the ion trap blades shown in our trap photograph and we thank Martin Lichtman for a thorough reading of the manuscript.

-
- [1] Philipp Schindler, Daniel Nigg, Thomas Monz, Julio T Barreiro, Esteban Martinez, Shannon X Wang, Stephan Quint, Matthias F Brandl, Volckmar Nebendahl, Christian F Roos, Michael Chwalla, Markus Hennrich, and Rainer Blatt. A quantum information processor with trapped ions. *New Journal of Physics*, 15(12):123012, 2013.
- [2] D J Szwer, S C Webster, A M Steane, and D M Lucas. Keeping a single qubit alive by experimental dynamic decoupling. *Journal of Physics B: Atomic, Molecular and Optical Physics*, 44(2):025501, 2011.
- [3] C. Langer, R. Ozeri, J. D. Jost, J. Chiaverini, B. DeMarco, A. Ben-Kish, R. B. Blakestad, J. Britton, D. B. Hume, W. M. Itano, D. Leibfried, R. Reichle, T. Rosenband, T. Schaetz, P. O. Schmidt, and D. J. Wineland. Long-lived qubit memory using atomic ions. *Phys. Rev. Lett.*, 95:060502, Aug 2005.
- [4] D. Kielpinski, C. Monroe, and D. J. Wineland. Architecture for a large-scale ion-trap quantum computer. *Nature*, 417(6890):709–711, June 2002.
- [5] C. Monroe, D. M. Meekhof, B. E. King, and D. J. Wineland. A “schrödinger cat” superposition state of an atom. *Science*, 272(5265):1131–1136, 1996.
- [6] Thomas Monz, Philipp Schindler, Julio T. Barreiro, Michael Chwalla, Daniel Nigg, William A. Coish, Maximilian Harlander, Wolfgang Hänsel, Markus Hennrich, and Rainer Blatt. 14-qubit entanglement: Creation and coherence. *Phys. Rev. Lett.*, 106:130506, Mar 2011.
- [7] C. Monroe, R. Raussendorf, A. Ruthven, K. R. Brown, P. Maunz, L.-M. Duan, and J. Kim. Large-scale modular quantum-computer architecture with atomic memory and photonic interconnects. *Phys. Rev. A*, 89:022317, Feb 2014.
- [8] D. L. Moehring, P. Maunz, S. Olmschenk, K. C. Younge, D. N. Matsukevich, L.-M. Duan, and C. Monroe. Entanglement of single-atom quantum bits at a distance. *Nature Physics*, 449:68–71, September 2007.
- [9] B.B. Blinov, D. L. Moehring, L.-M. Duan, and C. Monroe. Observation of entanglement between a single trapped atom and a single photon. *Nature Physics*, 428:153–157, March 2004.
- [10] S. Olmschenk, D. N. Matsukevich, P. Maunz, D. Hayes, L.-M. Duan, and C. Monroe. Quantum teleportation between distant matter qubits. *Science*, 323(5913):486–489, 2009.
- [11] B. Hensen, H. Bernien, A. E. Dreau, A. Reiserer, N. Kalb, M. S. Blok, J. Ruitenbergh, R. F. L. Vermeulen, R. N. Schouten, C. Abellan, W. Amaya, V. Pruneri, M. W. Mitchell, M. Markham, D. J. Twitchen, D. Elkouss, S. Wehner, T. H. Taminiau, and R. Hanson. Loophole-free bell inequality violation using electron spins separated by 1.3 kilometres. *Nature Physics*, 526:682686, October 2015.
- [12] William Wootters and Wojciech Zurek. A single quantum cannot be cloned. *Nature*, 299:802, 1982.
- [13] H.-J. Briegel, W. Dür, J. I. Cirac, and P. Zoller. Quantum repeaters: The role of imperfect local operations in quantum communication. *Phys. Rev. Lett.*, 81:5932–5935, Dec 1998.
- [14] Prem Kumar. Quantum frequency conversion. *Opt. Lett.*,

- 15(24):1476–1478, Dec 1990.
- [15] A. G. Radnaev, Y. O. Dudin, R. Zhao, H. H. Jen, S. D. Jenkins, A. Kuzmich, and T. A. B. Kennedy. A quantum memory with telecom-wavelength conversion. *Nature Physics*, 6:894899, September 2010.
- [16] H. J. McGuinness, M. G. Raymer, C. J. McKinstrie, and S. Radic. Quantum frequency translation of single-photon states in a photonic crystal fiber. *Phys. Rev. Lett.*, 105:093604, Aug 2010.
- [17] Matthew T. Rakher, Lijun Ma, Oliver Slattery, Xiao Tang, and Kartik Srinivasan. Quantum transduction of telecommunications-band single photons from a quantum dot by frequency upconversion. *Nature Photonics*, 4:786791, October 2010.
- [18] J. S. Pelc, L. Ma, C. R. Phillips, Q. Zhang, C. Langrock, O. Slattery, X. Tang, and M. M. Fejer. Long-wavelength-pumped upconversion single-photon detector at 1550 nm: performance and noise analysis. *Opt. Express*, 19(22):21445–21456, Oct 2011.
- [19] Sebastian Zaske, Andreas Lenhard, Christian A. Keßler, Jan Kettler, Christian Hepp, Carsten Arend, Roland Albrecht, Wolfgang-Michael Schulz, Michael Jetter, Peter Michler, and Christoph Becher. Visible-to-telecom quantum frequency conversion of light from a single quantum emitter. *Phys. Rev. Lett.*, 109:147404, Oct 2012.
- [20] Boris Albrecht, Pau Farrera, Matteo Fernandez-Gonzalvo, Xavier ad Cristiani, and Hugues de Riedmatten. A waveguide frequency converter connecting rubidium-based quantum memories to the telecom c-band. *Nature Communications*, 5:337, 2014.
- [21] Serkan Ates, Imad Agha, Angelo Gulinatti, Ivan Rech, Matthew T. Rakher, Antonio Badolato, and Kartik Srinivasan. Two-photon interference using background-free quantum frequency conversion of single photons emitted by an inas quantum dot. *Phys. Rev. Lett.*, 109:147405, Oct 2012.
- [22] Edo Waks and C. Monroe. Protocol for hybrid entanglement between a trapped atom and a quantum dot. *Phys. Rev. A*, 80:062330, Dec 2009.
- [23] J. J. Bollinger, D. J. Heinzen, W. M. Itano, S. L. Gilbert, and D. J. Wineland. A 303 MHz frequency standard based on trapped be^+ ions. *IEEE T. Instrum. Meas.*, 40(2):126–128, April 1991.
- [24] P. T. H Fisk, M. J. Sellars, M. A. Lawn, and G. Coles. Accurate measurement of the 12.6 GHz ‘clock’ transition in trapped 171Yb^+ ions. *IEEE T. Ultrason. Ferr.*, 44(2):344–345, March 1997.
- [25] S. Debnath, N. M. Linke, K. A. Figgatt, C. Landsman, K. Wright, and C. Monroe. Demonstration of a small programmable quantum computer with atomic qubits. *Nature Physics*, 536:63–66, August 2016.
- [26] H. Häffner, C. F. Roos, and R. Blatt. Quantum computing with trapped ions. *Physics Reports*, 469(4):155–203, December 2008.
- [27] J. Smith, A. Lee, P. Richerme, B. Neyenhuis, P. W. Hess, P. Hauke, M. Heyl, Huse D.A., and C. Monroe. Many-body localization in a quantum simulator with programmable random disorder. *Nature Physics*, May 2016.
- [28] P. A. Ivanov, S. S. Ivanov, N. V. Vitanov, A. Mering, M. Fleischhauer, and K. Singer. Simulation of a quantum phase transition of polaritons with trapped ions. *Phys. Rev. A: At., Mol., Opt. Phys.*, 80(6):060301, December 2009.
- [29] D. Porras and J. I. Cirac. Effective quantum spin systems with trapped ions. *Phys. Rev. Lett.*, 92(20):207901, May 2004.
- [30] R. Blatt and C. F. Roos. Quantum simulations with trapped ions. *Nature Physics*, 8:277–284, February 2012.
- [31] L.-M. Duan and C. Monroe. *Colloquium* : Quantum networks with trapped ions. *Rev. Mod. Phys.*, 82:1209–1224, Apr 2010.
- [32] P. Maunz, S. Olmschenk, D. Hayes, D. N. Matsukevich, L.-M. Duan, and C. Monroe. Heralded quantum gate between remote quantum memories. *Phys. Rev. Lett.*, 102:250502, Jun 2009.
- [33] A. Stute, B. Casabone, P. Schindler, T. Monz, P. O. Schmidt, B. Brandstatter, T. E. Northup, and R. Blatt. Demonstration of a small programmable quantum computer with atomic qubits. *Nature Physics*, 485:482–485, May 2012.
- [34] L.-M. Duan, M. J. Madsen, D. L. Moehring, P. Maunz, R. N. Kohn, and C. Monroe. Probabilistic quantum gates between remote atoms through interference of optical frequency qubits. *Phys. Rev. A*, 73:062324, Jun 2006.
- [35] D. Hucul, I. V. Inlek, G. Vittorini, C. Crocker, S. Debnath, S. M. Clark, and C. Monroe. Modular entanglement of atomic qubits using photons and phonons. *Nature Physics*, 11:37–42, January 2015.
- [36] P. Maunz, D. L. Moehring, S. Olmschenk, K. C. Younge, D. N. Matsukevich, and C. Monroe. Quantum interference of photon pairs from two remote trapped atomic ions. *Nature Physics*, 3:538–541, June 2007.
- [37] Carolyn Aughter, Chen-Kuan Chou, Thomas W. Noel, and Boris B. Blinov. Ion-photon entanglement and bell inequality violation with 138ba^+ . *J. Opt. Soc. Am. B*, 31(7):1568–1572, Jul 2014.
- [38] L. Slodička, G. Hétet, N. Röck, P. Schindler, M. Henrich, and R. Blatt. Atom-atom entanglement by single-photon detection. *Phys. Rev. Lett.*, 110:083603, Feb 2013.
- [39] P. K. Ghosh. *Ion Traps*. Oxford University Press, 1996.
- [40] M. J. Madsen, W. K. Hensinger, D. Stick, J. A. Rabchuk, and C. Monroe. Planar ion trap geometry for microfabrication. *Appl. Phys. B: Lasers Opt.*, 78(5):639–651, March 2004.
- [41] D Munshi, D, Dutta, T, Rebhi, and R Mukherjee M. Precision measurement of branching fractions of $^{138}\text{ba}^+$: Testing many-body theories below the 1% level. *Phys. Rev. A*, 91:040501, Apr 2015.
- [42] Richard Jozsa. Fidelity for mixed quantum states. *Journal of Modern Optics*, 41(12):2315–2323, 1994.
- [43] B. Casabone, K. Friebe, B. Brandstätter, K. Schüppert, R. Blatt, and T. E. Northup. Enhanced quantum interface with collective ion-cavity coupling. *Phys. Rev. Lett.*, 114:023602, Jan 2015.
- [44] Stephen Begley, Markus Vogt, Gurpreet Kaur Gulati, Hiroki Takahashi, and Matthias Keller. Optimized multi-ion cavity coupling. *Phys. Rev. Lett.*, 116:223001, May 2016.
- [45] Erik W. Streed, Benjamin G. Norton, Andreas Jechow, Till J. Weinhold, and David Kielpinski. Imaging of trapped ions with a microfabricated optic for quantum information processing. *Phys. Rev. Lett.*, 106:010502, Jan 2011.
- [46] G Shu, M R Dietrich, N Kurz, and B B Blinov. Trapped ion imaging with a high numerical aperture spherical mirror. *Journal of Physics B: Atomic, Molecular and Optical Physics*, 42(15):154005, 2009.
- [47] Karan K. Mehta, Colin D. Bruzewicz, Robert McConnell,

- Rajeev J. Ram, Jeremy M. Sage, and John Chiaverini. Integrated optical addressing of an ion qubit. *Nature Nanotechnology*, August 2016.
- [48] H. Bernien, B. Hensen, W. Pfaff, G. Koolstra, M. S. Blok, L. Robledo, T. H. Taminiau, M. Markham, D. J. Twitchen, L. Childress, and R. Hanson. Heralded entanglement between solid-state qubits separated by three metres. *Nature Physics*, 497:86–90, April 2013.
- [49] Serkan Ates, Imad Agha, Angelo Gulinatti, Ivan Rech, Matthew T. Rakher, Antonio Badolato, and Kartik Srinivasan. Two-photon interference using background-free quantum frequency conversion of single photons emitted by an inas quantum dot. *Phys. Rev. Lett.*, 109:147405, Oct 2012.
- [50] Z. Vernon, M. Liscidini, and J. E. Sipe. Quantum frequency conversion and strong coupling of photonic modes using four-wave mixing in integrated microresonators. *Phys. Rev. A*, 94:023810, Aug 2016.
- [51] C. J. McKinstrie, J. D. Harvey, S. Radic, and M. G. Raymer. Translation of quantum states by four-wave mixing in fibers. *Opt. Express*, 13(22):9131–9142, Oct 2005.
- [52] Qing Li, Marcelo Davano, and Kartik Srinivasan. Efficient and low-noise single-photon-level frequency conversion interfaces using silicon nanophotonics. *Nature Photonics*, 10:406–414, April 2016.
- [53] Robert Boyd. *Nonlinear Optics*. Academic Press, 2008.
- [54] Krishnan R. Parameswaran, Roger K. Route, Jonathan R. Kurz, Rostislav V. Roussev, Martin M. Fejer, and Masatoshi Fujimura. Highly efficient second-harmonic generation in buried waveguides formed by annealed and reverse proton exchange in periodically poled lithium niobate. *Opt. Lett.*, 27(3):179–181, Feb 2002.
- [55] Helge Rütz, Kai-Hong Luo, Hubertus Suche, and Christine Silberhorn. Towards a quantum interface between telecommunication and uv wavelengths: design and classical performance. *Applied Physics B*, 122(1):1–8, 2016.
- [56] R. Clark, T. Kim, and J. Kim. Double-stage frequency down-conversion system for distribution of ion-photon entanglement over long distances. In *2011 IEEE Photonics Society Summer Topical Meeting Series*, pages 45–46, July 2011.
- [57] Ryan A. Clark. Quantum frequency conversion for ytterbium ion based quantum repeaters. Master’s thesis, Duke University, North Carolina, 2012.
- [58] John Wright, Carolyn Auchter, Chen-Kuan Chou, Richard D. Graham, Thomas W. Noel, Tomasz Sakrejda, Zichao Zhou, and Boris B. Blinov. Toward a scalable quantum computing architecture with mixed species ion chains. *Quantum Information Processing*, pages 1–11, 2016.
- [59] Christoph Simon and William T. M. Irvine. Robust long-distance entanglement and a loophole-free bell test with ions and photons. *Phys. Rev. Lett.*, 91:110405, Sep 2003.
- [60] A. G. Radnaev, Y. O. Dudin, R. Zhao, H. H. Jen, S. D. Jenkins, A. Kuzmich, and T. A. B. Kennedy. A quantum memory with telecom-wavelength conversion. *Nat Phys*, 6(11):894–899, Nov 2010.
- [61] Vahid Esfandyarpour, Carsten Langrock, and Martin Fejer. Cascaded downconversion interface to the telecom band for single-photon-level signals at 650 nm. In *Conference on Lasers and Electro-Optics*, page FTh4A.4. Optical Society of America, 2016.
- [62] X. Li, J. Sivers, Z. Zhou, and Q. Quraishi. Quantum freq. conversion for telecom photon generation from ba+ ion. *Philosophical Transactions A*, 2016.
- [63] Adriana E. Lita, Aaron J. Miller, and Sae Woo Nam. Counting near-infrared single-photons with 95% efficiency. *Opt. Express*, 16(5):3032–3040, Mar 2008.